Struct Chem
DOI 10.1007/s11224-016-0856-0

ORIGINAL RESEARCH

Supramolecular solid-state structure, potential energy surfaces and evaluation of antiproliferative effect of 2-benzothiazolylhydrazone derivatives in vitro

Robert Katava[1] · Sandra Kraljević Pavelić[2] · Anja Harej[2] · Tomica Hrenar[3] · Gordana Pavlović[1]

Received: 22 July 2016 / Accepted: 22 September 2016

Abstract The in situ condensation reaction of 2-hydrazinobenzothiazole with salicylaldehyde, 3,4-dihydroxybenzaldehyde, 2,4-dihydroxybenzaldehyde, 2,5-dihydroxybenzaldehyde, 2,3-dihydroxybenzaldehyde, 2-hydroxy-1-naphthaldehyde, 2-methoxy-1-naphthaldehyde, 4-methoxy-1-naphthaldehyde and 6-methoxy-2-naphthaldehyde produced 9 hydrazone Schiff bases (L1–L9, respectively) which were identified and characterized by elemental analysis, IR and NMR spectroscopy. The crystal and molecular structures of four Schiff bases (L1, L7–L9) have been determined by the single-crystal X-ray diffraction method confirming the imino form of L1 and the amino tautomeric form of L7–L9 compounds. Molecular structure analysis also confirmed that reported compounds are *E*-isomers relative to exo C = N imino bond. The $N_{hydrazino}$–H group of amino tautomers forms $N_{hydrazino}$–H···$N_{thiazolyl}$ intermolecular hydrogen bonds shaping molecules into $R_2^2(8)$ rings, while imino tautomer of L1 forms $C(4)$ infinite helical chains via $N_{thiazolyl}$–H···$N_{hydrazino}$ type of intermolecular hydrogen bond. The methoxy group (L7–L9) further shaped these primary supramolecular synthons into different supramolecular arrangements via C–H···O, C–H···N and C–H···S intermolecular hydrogen bonds. The role of aryl substituents in the shaping and stabilization of supramolecular architectures of L1, L7–L9 is supported by quantum chemical calculations. Strong antiproliferative effects on tumor cells and cytotoxic effects on fibroblasts are shown for all ligands L1–L9 with exception of L6 and L7 that had no effect on fibroblast cells.

Keywords Schiff base ligands · Hydrazones · Benzothiazoles · Antiproliferative activity

Introduction

Among heterocyclic compounds, 1,3-benzothiazoles gained special attention due to diverse biological activities and capability to bind to DNA molecules via π–π interactions. This results in antitumor, antimicrobial, antidiabetic, anticonvulsant and anti-inflammatory activity [1–6]. Moreover, the hydrazone functional group (–C = N–NH–) is of great importance in medicinal chemistry with a potential in diverse applications. Combining hydrazone and benzothiazole functionalities in a unique molecular system (Bzt–NH–N = CH–Aryl; Bzt = benzothiazolyl) may thus bring new properties and synergistic effects in both structural and electronic context.

Hydrazone Schiff bases as ligands have vast and diverse coordination potential to metal center due to stereochemically suitable positions of donating atoms including: endocyclic nitrogen, imine and hydrazone nitrogen atom and other functionalities at aryl moiety. Biological effects of 2-hydrazinobenzothiazole Schiff base metal complexes are still a promising area of research, particularly in comparison with uncoordinated ligands effects since increased

Electronic supplementary material The online version of this article (doi:10.1007/s11224-016-0856-0) contains supplementary material, which is available to authorized users.

✉ Gordana Pavlović
gpavlovic@ttf.hr

[1] Department of Applied Chemistry, Faculty of Textile Technology, University of Zagreb, Prilaz baruna Filipovića 28a, 10000 Zagreb, Croatia

[2] Department of Biotechnology, Centre for High-throughput Technologies, University of Rijeka, Radmile Matejčić 2, 51000 Rijeka, Croatia

[3] Department of Chemistry, Faculty of Science, University of Zagreb, Horvatovac 102a, 10000 Zagreb, Croatia

Published online: 01 October 2016

biological activity is noticed when organic drugs are administered in the form of metal complex. Also, their applications are versatile including not only medicinal, but supramolecular chemistry and chemistry of dyes [7].

Survey of CSD [8, 9] revealed 12 structures of uncoordinated 2-hydrazinobenzothiazole Schiff bases that can be found in more common amino [10, 11] or just one so far imino tautomeric form [11] (Scheme 1), as solvates and anhydrous compounds. The preferential supramolecular architecture of hydrazones in the solid state is simultaneously dependable of the type and position of the substituents on the aryl moiety and the presence of solvate molecules in the crystal, rather than of the tautomeric type of hydrazone molecule.

In the more common amino hydrazones [10, 11], intermolecular contacts are characterized by $N_{hydrazino}$–H···$N_{thiazolyl}$ hydrogen bonds that either form symmetric $R_2^2(8)$ dimers or infinite helical $C(4)$ chains that are often supported by π···π interactions. In solvated compounds, solvate molecules are involved in indirect links between the hydrazone molecules [11].

In our effort to prepare metal complexes and investigate their pharmacological activities, we synthesized and characterized a series of nine ligands (L1–L9) functionalized by −OH or $-OCH_3$ functionalities at different phenyl or naphthyl positions (Bzt–NH–N = CH–C_6H_4–R_1R_2; Bzt–NH–N = CH–$C_{10}H_7$–R_3 (Scheme 2) with the aim to (a) enhance coordination capability of 2-benzothiazolylhydrazone derivatives as ligands and (b) outline supramolecular architecture of these ligands in uncoordinated state and (c) test antiproliferative effects of obtained structures in vitro.

The synthesis of six ligands (L1–L6) was previously reported [12–15]. All tested compounds were identified by elemental analysis, IR spectroscopy, NMR spectroscopy, and additionally, compounds L1, L7–L9 were characterized by single-crystal X-ray diffraction method. Structural and theoretical studies in the solid state were performed in order to identify any common features of intermolecular interactions that might be responsible for biological activity of these ligand systems. In the continuation of our research, we plan to prepare metal complexes of these ligands and investigate their biological activity as well.

Experimental

Materials and methods

Salicylaldehyde, 3,4-dihydroxybenzaldehyde, 2,4-dihydroxybenzaldehyde, 2,5-dihydroxybenzaldehyde, 2,3-dihydroxybenzaldehyde, 2-hydroxy-1-naphthaldehyde, 2-methoxy-1-naphthaldehyde, 4-methoxy-1-naphthaldehyde, 6-methoxy-2-naphthaldehyde and 2-hydrazinobenzothiazole were purchased from commercial sources Acros Organics and Sigma-Aldrich and used as received. Infrared spectra were recorded on a PerkinElmer FT-IR spectrometer Spectrum TWO equipped with a PerkinElmer Universal ATR Sampler Accessory in the 4000–400 cm^{-1} region. The ^1H NMR and the ^{13}C NMR spectra were recorded on a Brucker Avance 600 MHz NMR Spectrometer (600 and 150 MHz, for ^1H and ^{13}C, respectively) in DMSO-d_6 solutions. Chemical shifts are reported in ppm relative to TMS as an internal standard. The elemental analysis was performed at the Analytical Services Laboratory of the Ruđer Bošković Institute, Zagreb, on a Perkin Elmer CHNS/O analyzer Series II 2400. Melting points were determined on a Reichert Austria 7905 microscope for the determination of the melting points. The powder X-ray diffraction data were collected by the Panalytical X'Change powder diffractometer in the Bragg–Brentano geometry using CuKα radiation. The sample was contained on a Si sample holder. Patterns were collected in the range of $2\theta = 5$–$50°$ with the step size of 0.03° and at 1.5 s per step. The data were collected using the X'Pert programs Suite [16] and visualized using the DiffractWD [17].

Preparative and crystallization procedures

2-Benzothiazolylhydrazone derivatives were prepared by condensation reactions of 2-hydrazinobenzothiazole (3 mmol) with appropriate arenealdehydes (3 mmol) in ethanol (30 mL) (Scheme 2). The mixture was refluxed for 4 h at 70 °C. Resulting precipitates were filtered off and washed with cold ethanol. The compounds L7–L9 were prepared according to the same synthetic procedure as previously reported L1–L6 [12–15]. Spectral data and elemental analysis of all prepared compounds can be found in the Supporting Information (Table S2, Figs. S1–S27).

Scheme 1 Tautomeric forms of 2-benzothiazolylhydrazones

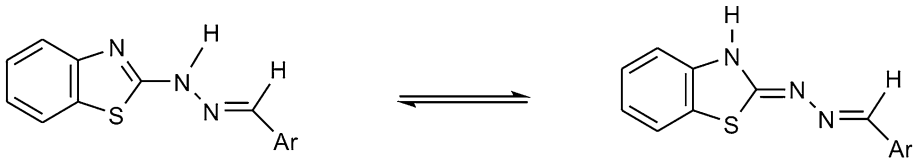

Crystals of 2-hydroxybenzaldehyde-(2-benzothiazolylhydrazone) (L1), 4-methoxy-1-naphthaldehyde-(2-benzothiazolylhydrazone) (L8) and 6-methoxy-2-naphthaldehyde-(2-benzothiazolylhydrazone) (L9) precipitated after a few days from cooled DMSO solutions. Crystals of 2-methoxy-1-naphthaldehyde-(2-benzothiazolylhydrazone) (L7) were prepared by evaporation of pyridine solution of L7.

2-methoxy-1-naphthaldehyde-(2-benzothiazolylhydrazone) (L7)

Yellow solid; yield: 85 %; m.p. 216–218 °C; IR (ν cm^{-1}, ATR): 3168 (N–H), 1608 (C = N), 1561 (C_{arom} = C_{arom}), 1270 (C_{arom}–N), 1248 (C–O); ^{1}H NMR (600.00 MHz, DMSO-d_6, δ ppm): 12.27 (s, 1H, NH), 9.31 (d, J = 8.70 Hz, 1H, H_{arom}), 8.93 (s, 1H, N = C–H), 8.02 (d, J = 9.06 Hz, 1H, H_{arom}), 7.92 (d, J = 8.10 Hz, 1H, H_{arom}), 7.83 (d, J = 7.74 Hz, 1H, H_{arom}), 7.67 (t, J = 7.74 Hz, 1H, H_{arom}), 7.52–7.46 (m, 3H, H_{arom}), 7.34 (t, J = 7.44 Hz, 1H, H_{arom}), 7.14 (t, J = 7.68 Hz, 1H, H_{arom}), 4.01 (s, 3H, CH_3); ^{13}C NMR (150.00 MHz, DMSO-d_6, δ ppm) 166.9, 157.3, 132.2, 130.5, 128.8, 128.6, 128.2, 125.9, 125.4, 124.0, 121.5, 114.3, 113.4, 56.7; Anal. calcd. for $C_{19}H_{15}N_3OS$: C, 68.44; H, 4.54; N, 12.61; S, 9.62 %, Found: C, 68.30; H, 4.74; N, 12.81; S, 9.73 %.

4-methoxy-1-naphthaldehyde-(2-benzothiazolylhydrazone) (L8)

Yellow solid; yield: 77 %; m.p. 219–221 °C; IR (ν cm^{-1}, ATR): 3170 (N–H), 1609 (C = N)$_{exo}$, 1560 (C_{arom} = C_{arom}), 1268 (C_{arom}–N), 1228 (C–O); ^{1}H NMR (600.00 MHz, DMSO-d_6, δ ppm): 12.14 (s, 1H, NH), 9.02 (d, J = 8.46 Hz, 1H, H_{ar}), 8.68 (s, 1H, N = C–H), 8.30 (d, J = 8.34 Hz, 1H, H_{arom}), 7.82–7.80 (m, 2H, H_{arom}), 7.74 (m, J = 7.56 Hz, 1H, H_{arom}) 7.62 (t, J = 7.44 Hz, 1H, H_{arom}), 7.46 (d, J = 7.98 Hz, 1H, H_{ar}), 7.33 (t, J = 7.56 Hz, 1H, H_{arom}), 7.13–7.08 (m, 2H, H_{arom}), 4.05 (s, 3H, CH_3); ^{13}C NMR (150.00 MHz, DMSO-d_6, δ ppm): 166.8, 156.3, 130.8, 129.9, 127.8, 125.9, 125.7, 125.1, 124.6, 122.1, 121.5, 121.4, 104.3, 55.8; Anal. calcd. for $C_{19}H_{15}N_3OS$: C, 68.44; H, 4.54; N, 12.61; S, 9.62 %, Found: C, 68.33; H, 4.70; N, 12.71; S, 9.65 %.

6-methoxy-2-naphthaldehyde-(2-benzothiazolylhydrazone) (L9)

Yellow solid; yield (based on 2-hydrazinobenzothiazole): 79 %; m.p. 235–237 °C; IR (ν cm^{-1}, ATR): 3183 (N–H), 1621 (C = N)$_{exo}$, 1601 (C = N)$_{endo}$, 1574 (C_{arom} = C_{arom}), 1265 (C_{arom}–N), 1243 (C–O); ^{1}H NMR

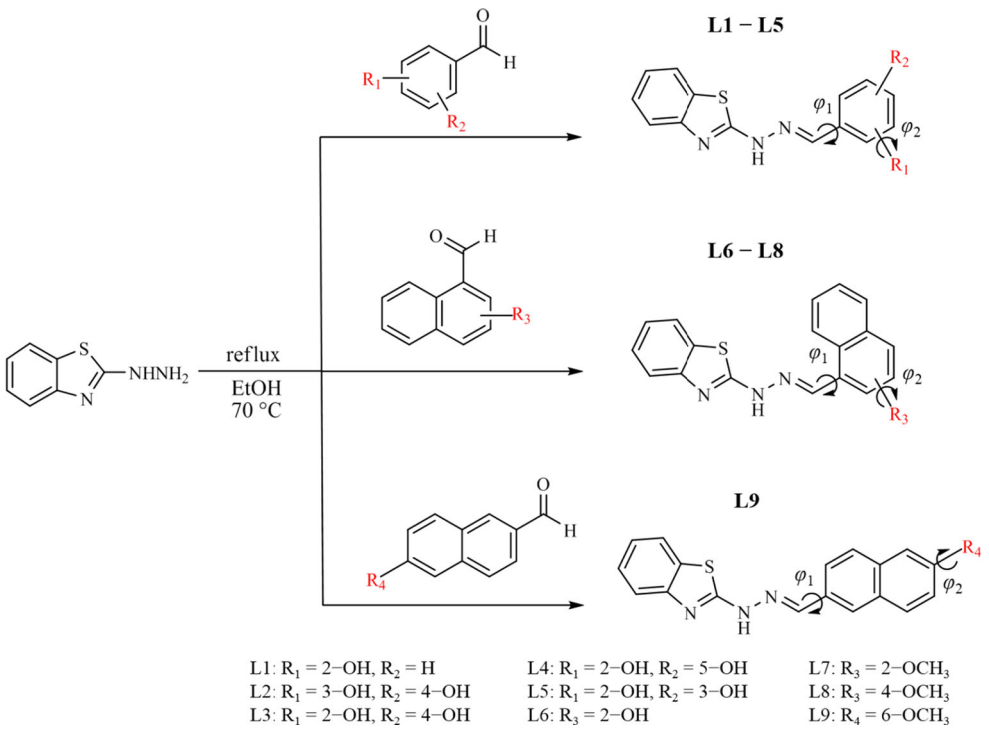

Scheme 2 Preparation and structural formulas of compounds L1–L9 with torsional coordinates φ_1 and φ_2 (atoms that define torsional coordinates are presented in Fig. S28)

(600.00 MHz, DMSO-d_6, δ ppm) 12.25 (s, 1H, NH), 8.30 (s, 1H, N = C–H), 8.02 (s, 1H, H_{arom}) 7.95 (d, J = 8.46 Hz, 1H, H_{arom}), 7.89 (t, J = 8.58 Hz, 2H, H_{arom}), 7.80 (d, J = 7.56 Hz, 1H, H_{arom}), 7.49 (d, J = 7.62 Hz, 1H, H_{arom}), 7.36–7.33 (m, 2H, H_{arom}), 7.23 (d, J = 8.04 Hz, 1H, H_{arom}), 7.14 (t, J = 6.96 Hz, 1H, H_{arom}), 3.91 (s, 3H, CH_3); ^{13}C NMR (150.00 MHz, DMSO-d_6, δ ppm) 167.0, 158.1, 135.0, 129.8, 129.8, 128.2, 127.8, 127.4, 125.9, 122.8, 121.5, 119.0, 106.4, 55.3; Anal. calcd. for $C_{19}H_{15}N_3OS$: C, 68.44; H, 4.54; N, 12.61; S, 9.62 %, Found: C, 68.51; H, 4.71; N, 12.72; S, 9.70 %.

Single-crystal X-ray diffraction experiment

The general and crystallographic data for compounds L1, L7–L9 are listed in Table 1. Crystallographic data were recorded on Oxford Xcalibur diffractometer, equipped with a CCD area detector, using Mo Kα radiation (λ = 0.71,073 Å) at T = 296 K for L1, L7 and L9 and on Oxford Diffraction Xcalibur Nova R, equipped with a CCD area detector, using Cu Kα radiation (λ = 1.54,184 Å) at T = 296 K for L8. Programs CrysAlis CCD [18] and CrysAlis RED [18] (Version 1.171.37.35) were employed for data collection, cell refinement and data reduction. Structures were solved by direct methods, and all non-hydrogen atoms were refined anisotropically based on F^2 by weighted full-matrix least squares. Programs SHELXST-2014 [19] and SHELXL-2014 [19] integrated in the WinGX v. 2014.1.v [20] software system were used to solve and refine structures. Hydrogen atoms belonging to Csp^2 and Csp^3 carbon atoms were placed in geometrically idealized positions, and they were constrained to ride on their parent atoms using the appropriate SHELXL-2014 [19] HFIX instructions. The positions of hydrogen atoms belonging to the oxygen O1 and nitrogen N1 in compound L1, nitrogen N2 in compound L8 and nitrogen atoms N21 and N22 in compounds L7 and L9 were determined from difference Fourier syntheses, and their coordinates were refined freely, while isotropic displacement parameters were refined with $U_{iso}(H) = 1.2\ U_{eq}(N)$. The molecular geometry calculations were performed by PLATON [21], and the molecular graphics were generated using Mercury program [22].

Table 1 General and crystal data and summary of intensity data collection and structure refinement for compounds L1, L7–L9

Compound	L1	L7	L8	L9
Brutto chemical formula	$C_{14}H_{11}N_3OS$	$C_{19}H_{15}N_3OS$	$C_{19}H_{15}N_3OS$	$C_{19}H_{15}N_3OS$
M_r	269.3	333.4	333.4	333.4
Crystal system, color, habit	Monoclinic, yellow, prism	Monoclinic, yellow, prism	Monoclinic, yellow, prism	Monoclinic, yellow, needle
Space group	$P\ 2_1/n$	$I\ 2/a$	$P\ 2_1/n$	$P\ 2_1/c$
Crystal dimensions (mm^3)	0.49 × 0.16 × 0.10	0.35 × 0.23 × 0.20	0.37 × 0.20 × 0.12	0.62 × 0.17 × 0.08
Unit cell parameters				
a/Å	15.6365 (10)	21.0027 (12)	12.0230 (2)	17.5548 (10)
b/Å	4.5903 (3)	12.2101 (6)	6.3698 (1)	7.3052 (3)
c/Å	17.6379 (13)	24.9320 (14)	20.7480 (2)	26.3033 (15)
β/°	91.813 (6)	99.759 (5)	93.318 (1)	107.263 (6)
V/Å^3	1265.35 (3)	6301.2 (6)	1586.30 (1)	3221.2 (3)
$3Z$	4	16	4	8
ρ(calculated)/g cm^{-3}	1.41	1.41	1.40	1.37
μ/mm^{-1}	0.250	0.216	1.894	0.211
F(000)	560	2784	696	1392
θ–range/°	4.6–27.5	4.2–27.5	4.1–70.0	4.3–27.5
Reflections collected, unique ($R_{int.}$), observed [$I > 2\sigma(I)$]	5702, 2875, 1718	14,250, 7203, 3690	13,595, 3009, 2866	15,369, 7376, 4334
Number of parameters refined	178	441	221	441
$R(F_0)$	0.060	0.068	0.035	0.073
$R_w(F_0^2)$	0.112	0.092	0.100	0.117
Goodness of fit on F^2, S	0.986	1.004	1.071	1.038
Max. and min. electron density, $\Delta\rho_{max}$, $\Delta\rho_{min}$/e Å^{-3}	−0.222, 0.245	−0.241, 0.215	−0.259, 0.197	−0.281, 0.222

Cell culturing

Cell lines HeLa (cervical carcinoma), SW620 (colorectal adenocarcinoma, metastatic), HepG2 (hepatocellular carcinoma), A549 (lung adenocarcinoma) and 3T3 (mouse embryonic fibroblasts) were cultured as monolayers and maintained in Dulbecco's modified Eagle medium (DMEM) supplemented with 10 % fetal bovine serum (FBS), 2 mM L-glutamine, 100 U/ml penicillin and 100 μg/ml streptomycin in a humidified atmosphere with 5 % CO_2 at 37 °C.

Proliferation assays

The panel cell lines were inoculated onto a series of standard 96-well microtiter plates on day 0, at 5000 cells per well according to the doubling times of specific cell line. Test agents were then added in five, 10-fold dilutions (0.01–100 μM) and incubated for further 72 h. Working dilutions were freshly prepared on the day of testing in the growth medium. The solvent (DMSO) was also tested for eventual inhibitory activity by adjusting its concentration to be the same as in the working concentrations (DMSO concentration never exceeded 0.1 %). After 72 h of incubation, the cell growth rate was evaluated by performing the MTT assay: experimentally determined absorbance values were transformed into a cell percentage growth (PG) using the formulas proposed by NIH and described previously (1). This method compares the growth of treated cells with the growth of untreated cells in control wells on the same plate in comparison with the starting cell number values. Results are therefore a percentile difference from the calculated expected value.

The IC_{50} values for each compound were calculated from dose–response curves using linear regression analysis by fitting the mean test concentrations that give PG values above and below the reference value. If, however, all of the tested concentrations produce PGs exceeding the respective reference level of effect (e.g., PG value of 50) for a given cell line, the highest tested concentration is assigned as the default value (in the screening data report that default value is preceded by a " > " sign). Each test point was performed in quadruplicate in three individual experiments.

Quantum chemical calculation

Geometry optimization for ground states of monomers, dimers or tetramers was performed using hybrid functional B3LYP [23, 24] with D3 version of Grimme's dispersion [25] in combination with the 6-311 ++G(d,p) basis set. For all optimized structures, harmonic vibrational frequencies were calculated to insure that obtained geometries correspond to the minimum on the potential energy surface. Standard Gibbs energies of formation were calculated at $T = 298.15$ K and $p = 101{,}325$ Pa.

Potential energy surfaces (PES) scans for monomers were conducted by varying the torsional coordinates φ_1 and φ_2 (Scheme 2) using the automatic conformational generator implemented in program *qcc* [26, 27]. Data from PES scans were arranged in one- or two-way arrays. Parallelized combinatorial optimization algorithm for the arbitrary number of ways (dimensions) implemented in program *moon*ee [28] was used to determine all local minimums on the investigated PES. All local minimums were reoptimized at the B3LYP/6-311 ++G(d,p) level of the theory. All quantum chemical calculations were performed using the Gaussian 09 program [29].

Results and discussion

Chemistry

Target compounds were prepared in good yields by condensation reactions of 2-hydrazinobenzothiazole with appropriate arenealdehydes following a general procedure (Scheme 2). The proposed structural formulas of compounds L1, L7–L9 were verified by single-crystal X-ray diffraction, spectroscopic methods (FT-IR, ^{1}H and ^{13}C NMR) and elemental analysis. Compared to starting materials, the most notable changes in the IR spectra of prepared compounds are: disappearance of the absorption band at 3319 cm^{-1} assigned to $\nu(NH_2)$ of the 2-hydrazinobenzothiazole, disappearance of the absorption band in the 1631−1679 cm^{-1} region assigned to $\nu(C = O)$ of arenealdehydes and appearance of an intense band in the 1608–1621 cm^{-1} region assigned to the $\nu(C = N)$ of both imino functional group and benzothiazole moiety [30]. In compound L9 two medium intensity bands appear at 1621 and 1600 cm^{-1} and can be assigned to the $\nu(C = N)_{exo}$ of the imino functional group and to the $\nu(C = N)_{endo}$ of the benzothiazole moiety, respectively. IR spectra of compounds L7–L9 show weak intensity band in 3168−3183 cm^{-1} region assigned to ν(NH) and strong intensity band in the 1228–1248 cm^{-1} region assigned to ν(C–O) of the methoxy group. Condensation reactions of 2-hydrazinobenzothiazole with appropriate arenealdehydes are also confirmed with ^{1}H NMR spectral data. ^{1}H NMR spectra of compounds L7–L9 exhibit singlets in 12.14–12.27, 8.30−8.93 and 3.93−4.05 ppm regions assigned to the N–H, N = C–H and CH_3 protons, respectively. Compared to theoretically calculated values for monomeric compounds of benzothiazolyl hydrazones reported by Lindgren et al. [10], chemical shifts assigned to N–H protons, in the 12.14–12.27 ppm region, show

significant deshielding due to involvement of these protons in the formation of intermolecular hydrogen bonds. According to the literature data, chemical shifts assigned to N–H protons bond in the 9−12 ppm region are characteristic for *E*-isomeric form relative to exo C = N imino bond, contrary to chemical shift assigned to N–H protons in 14–15 ppm region found in *Z*-isomeric form [31, 32]. Accordingly, all prepared compounds (L7–L9) as well as previously reported (L1–L6) are *E*-stereoisomers. Calculated PXRD patterns of 2-benzothiazolylhydrazones L1 and L7 from the single-crystal X-ray crystallography studies, whose single crystals were obtained from DMSO (L1) and pyridine (L7) solutions, are in agreement with PXRD patterns of L1 and L7 prepared by condensation reactions in ethanol solutions (Supporting Information Figs. S29, S30).

Molecular structures of L1, L7–L9

Mercury–rendered ORTEP drawings of asymmetric units of compounds L1, L7−L9 are depicted in Fig. 1. Asymmetric units of compounds L1 and L8 consist of a single molecule, while asymmetric units of compounds L7 and L9 consist of two independent and conformationally slightly different molecules marked 1 and 2. The dihedral angle is calculated between the benzothiazolyl and arene plane. All compounds are moderately to strongly planar with dihedral angles between the benzothiazolyl [defined by atoms: S1, C1–C6, N1 and C7 (L1 and L8), S11, C11–C61, N11 and C71 (L7 and L9, molecule 1), and S12, C12–C62, N12 and C72 (L7 and L9, molecule 2)] and arene planes [defined by atoms: C9–C14 (L1), C9–C18 (L8), C91, C101–C181 (L7 and L9, molecule 1) and C92, C102–C182 (L7 and L9, molecule 2)] of: 5.41(15)° (L1), 9.96(5)° (L8), 4.47(11)° (L7, molecule 1), 8.82(10)° (L7, molecule 2), 3.37(8)° (L9, molecule 1), 6.03(9)° (L9, molecule 2). Molecular structure analysis also confirmed that reported compounds are *E*-isomers relative to exo C = N imino bond. Imino tautomeric form of L1 and amino form of L7–L9 has been confirmed by geometric parameters listed in Tables 2 and 3. The N1–C7 bond (1.335(3) Å) in L1 that exists in imino tautomeric form is predominantly σ in character and significantly longer in comparison with N1–C7 (L8), N11–C71 (L7, L9) and N12–C72 (L7, L9) bonds (1.294(3)–1.303(3) Å) in compounds L7–L9 that exist in amino form. The N2–C7 bond in L1 (1.299(3) Å) is predominantly π in character and significantly shorter in comparison with N2–C7 (L8), N21–C71 (L7, L9) and N22–C72 (L7, L9) bonds (1.346(4) Å–1.360(3) Å). The N3–C8 (L1, L8), N31–C81 (L7, L9) and N32–C82 (L7, L9) bonds are predominantly π in character (1.269(3)–1.290(3) Å) in all compounds. Values of selected bonds and angles in Tables 2 and 3 are in good agreement with values found in amino forms and one imino form of 2-benzothiazolylhydrazones reported by Nogueira et al. [11] (REFCODES: SAJQAX, SAJQEB, SAJQIF, SAJQOL, SAJQUR, SAJRAY, SAJREC, SAJRIG).

Intramolecular hydrogen bonds are found in structures L1, L7 and L8 (Table 4). Imino nitrogen atoms N3 (L1,

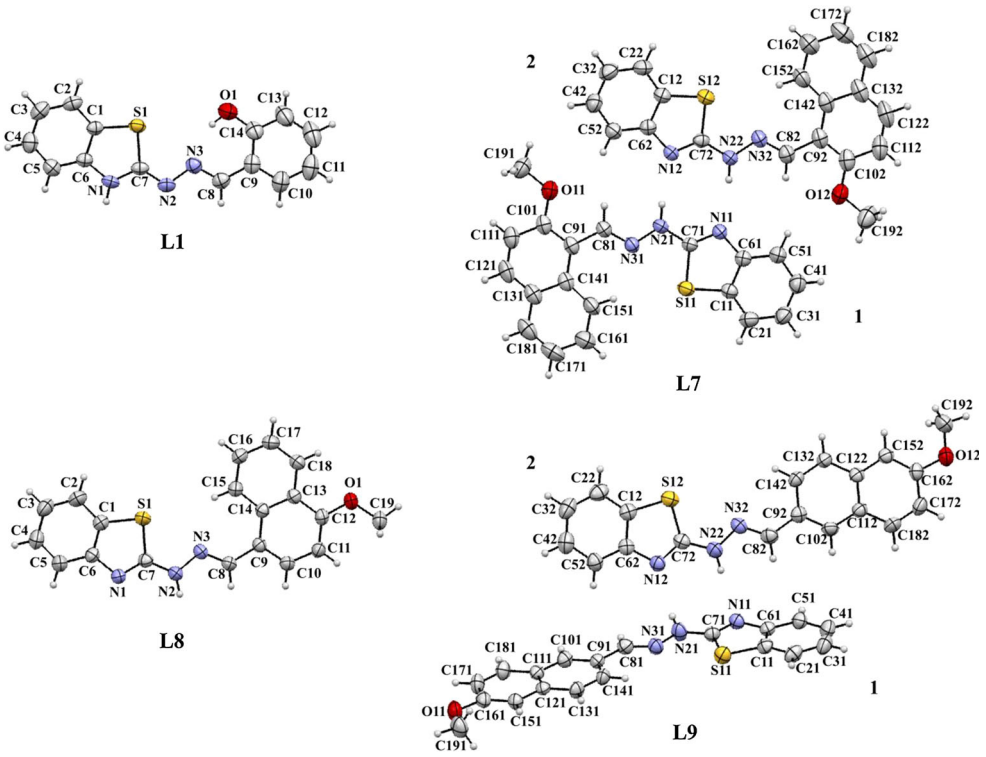

Fig. 1 Mercury–rendered ORTEP view of the molecular structure of compounds L1, L7–L9 showing the crystallographic atom-numbering scheme (the displacement ellipsoids are drawn at the 50 % probability level at 296(2) K, and the hydrogen atoms are drawn as *spheres* of arbitrary radius)

Table 2 Selected bond lengths (Å)

Compound	N1–C7	N2–C7	N2–N3	N3–C8
L1	1.335 (3)	1.299 (3)	1.389 (3)	1.290 (3)
L8	1.298 (2)	1.348 (2)	1.376 (2)	1.272 (2)
	N11–C71	N21–C71	N21–N31	N31–C81
L7	1.294 (3)	1.360 (3)	1.372 (3)	1.269 (3)
L9	1.303 (3)	1.353 (4)	1.372 (4)	1.281 (3)
	N12–C72	N22–C72	N22–N32	N32–C82
L7	1.299 (3)	1.350 (3)	1.382 (3)	1.275 (3)
L9	1.302 (3)	1.346 (4)	1.370 (3)	1.273 (4)

Table 3 Selected bond angles (°)

Compound	C6–N1–C7	C7–N2–N3	N2–N3–C8
L1	115.3 (2)	111.3 (2)	114.9 (2)
L8	109.7 (1)	115.1 (1)	116.4 (1)
	C61–N11–C71	C71–N21–N31	N21–N31–C81
L7	109.0 (2)	115.6 (2)	118.4 (2)
L9	109.2 (2)	117.1 (3)	115.5 (3)
	C62–N12–C72	C72–N22–N32	N22–N32–C82
L7	108.9 (2)	115.8 (2)	117.7 (2)
L9	109.4 (3)	120.4 (3)	114.9 (3)

L8), N31 (L7), N32 (L7) act as a proton acceptors and form strong O–H···N intramolecular hydrogen bond in L1 and weak C–H···N intramolecular hydrogen bond in L7 and L8. In all cases *S*(6) structural motif is formed by an intramolecular hydrogen bond.

Crystal structures of L1, L7–L9

2-hydroxybenzaldehyde-(2-benzothiazolylhydrazone) (L1)

Both intramolecular and intermolecular hydrogen bonds are present in the crystal structure of L1. Hydroxy O1 atom acts as a proton donor and forms intramolecular O1–H11O···N3 hydrogen bond with the imino N3 nitrogen atom, thus shaping *S*(6) structural motif. Bond length (2.656(3) Å) and <D–H···A angle (153(3) °) are in good agreement with corresponding O–H···N intramolecular hydrogen bond in structure of 2-benzothiazolylhydrazone reported by Nogueira et al. [11] (REFCODE: SAJREC). Intermolecular contacts are characterized by N–H···N hydrogen bonds (Fig. 2a, Table 4). Endocyclic N1 nitrogen atom acts as proton donor and forms N1–H11 N···N2 intermolecular hydrogen bond with hydrazone N2 nitrogen atom of the second molecule. Resulting supramolecular motif in the crystal structure of L1 is infinite helical *C*(4) chain generated via N1–H11 N···N2 hydrogen bond in the direction of the *b* axis (Fig. 2b). That alignment of

Table 4 Geometry of hydrogen bonds in compounds L1, L7–L9

D–H···A	D–H	H···A	D···A	<D–H···A	Symmetry code
L1					
O1–H11O···N3	0.84 (3)	1.88 (3)	2.656 (3)	153 (3)	
N1–H11 N···N2	0.83 (2)	2.05 (2)	2.877 (3)	174 (2)	1/2−x,1/2 + y,1/2−z
L7					
C151–H151···N31	0.93	2.25	2.900 (4)	126	
C152–H152···N32	0.93	2.28	2.929 (4)	127	
C51–H51···O12	0.93	2.63	3.461 (4)	150	
C52–H52···O11	0.93	2.63	3.478 (4)	150	
C151–H151···S11	0.93	2.92	3.831 (3)	168	
N21–H21N···N12	0.87 (2)	2.19 (2)	3.040 (3)	164 (2)	1/2−x,1/−y,1/2−z
N22–H22 N···N11	0.90 (2)	2.16 (2)	3.062 (3)	173 (2)	1/2−x,1/2−y,1/2−z
C22–H22···S11	0.93	2.97	3.683 (3)	135	x,−y + 1/2, + z+1/2
C192–H19F···N11	0.96	2.70	3.597 (4)	155	−x + 1/2, −y + 3/2, −z + 1/2
L8					
C15–H15···N3	0.93	2.31	2.9578 (18)	126	
N2–H12 N···N1	0.88 (2)	2.14 (2)	3.0104 (16)	173 (2)	2−x,−1−y,−z
C19–H19B···O1	0.96	2.54	3.440 (2)	156	1−x,2−y,−z
L9					
N21–H21 N···N12	0.86 (3)	2.25 (3)	3.040 (4)	155 (3)	1−x,1/2 + y,1/2−z
N22–H22 N···N11	0.85 (3)	2.28 (3)	3.110 (4)	169 (3)	1−x,−1/2 + y,1/2−z
C42–H42···O12	0.93	2.55	3.317 (4)	140	1 + x,1/2−y,1/2 + z

molecules in crystal is additionally supported by weak aromatic stacking interaction between the thiazolyl and phenyl rings of adjacent molecules (Table 5). Similar supramolecular helical arrangement is found in crystal structure of benzothiazolyl hydrazone reported by Lindgren et al. [10] (REFCODE: ZEZYUA).

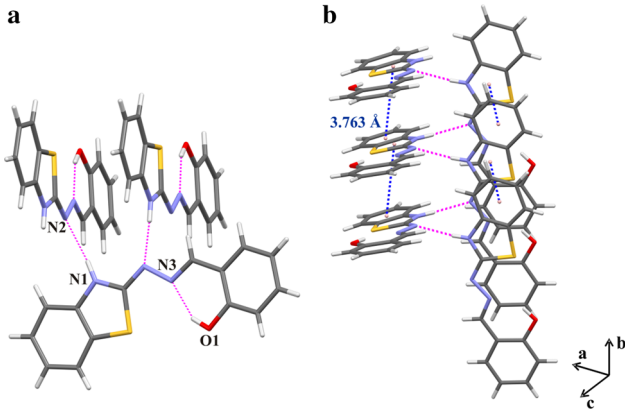

Fig. 2 **a** Main supramolecular motif in compound L1 formed by N1–H11 N···N2 intermolecular hydrogen bond and *S*(6) structural motif shaped via intramolecular O1–H11O···N3 hydrogen bond shown as *dashed magenta lines*. **b** Infinite helical *C*(4) chain in the direction of the *b* axis shaped via N1–H11 N···N2 hydrogen bond (shown as *dashed magenta lines*) and supported by weak aromatic stacking interaction between the thiazolyl and phenyl rings of adjacent molecules (shown as *dashed dark blue lines*)

2-methoxy-1-naphthaldehyde-(2-benzothiazolylhydrazone) (L7)

Weak intramolecular C151–H151···N31 and C152–H152···N32 hydrogen bonds that shape *S*(6) structural motif are present in independent molecules 1 and 2 in asymmetric unit of compound L7. Also, atom C151 (1) acts as a bifurcated proton donor and forms another intramolecular C151–H151···S11 hydrogen bond. Intermolecular contacts are characterized by N–H···N, C–H···O, C–H···N and C–H···S hydrogen bonds (Table 4). Hydrazino nitrogen atoms N21 and N22 act as proton donors and form intermolecular N21–H21 N···N12 and N22–H22 N···N11 hydrogen bonds that connect independent molecules 1 and 2 into $R_2^2(6)$ dimer (Fig. 3a). Independent molecules 1 and 2 are further mutually connected via weak C51–H51···O12 and C52–H52···O11 hydrogen bonds that form $R_2^2(22)$ rings. In the crystal structure, dimers are mutually connected via weak C192–H19F···N11 and C22–H22···S11 hydrogen bonds (Fig. 3b). The S11 atom acts as a bifurcated proton acceptor. Supramolecular architecture is additionally supported by π–π stacking (Table 5).

Table 5 Geometrical parameters of π···π interactions (Å, °) for compounds L1, L7 and L8

Interaction[a]	Cg···Cg distance	Cg···P1[b]	Cg···P2[c]	α[d]	β[e]	Slippage
L1						
Cg1–Cg2[i]	3.7627 (15)	3.4252 (10)	3.4598 (11)	1.34 (12)	23.1	1.479
Cg2–Cg1[ii]	3.7625 (15)	3.4598 (11)	3.4251 (10)	1.34 (12)	24.4	1.557
L7						
Cg1–Cg7	3.7916 (14)	3.3348 (10)	3.5423 (10)	11.15 (12)	20.9	1.352
Cg2–Cg8	3.9374 (18)	3.5156 (12)	3.6999 (12)	10.43 (14)	20.0	1.347
Cg8–Cg2	3.9373 (18)	3.6998 (12)	3.5155 (12)	10.43 (14)	26.8	1.773
Cg9–Cg3	3.7171 (19)	3.5295 (14)	3.4738 (12)	3.26 (15)	20.8	1.323
L8						
Cg1–Cg4[i]	3.8657 (8)	3.6310 (5)	3.6038 (6)	9.98 (7)	21.2	1.399
Cg4–Cg1[ii]	3.8657 (8)	3.6038 (6)	3.6310 (5)	9.98 (7)	20.1	1.326

[a] Ring Cg1 is defined by atoms S1, C1, C6, N1 and C7 (thiazolyl ring atoms) in L1 and L8 and by atoms S11, C11, C61, N11 and C71 (thiazolyl ring atoms) in L7. Cg2 is defined by atoms C1–C6 (phenyl ring atoms) in L1, and Cg3 is defined by atoms C91, C101–C141 (phenyl ring atoms) in L7. Cg4 is defined by atoms C13–C18 (phenyl ring atoms) in L8. Cg7 is defined by atoms S12, C12, C62, N12 and C72 (thiazolyl ring atoms) in L7. Cg8 is defined by atoms C12–C62 in L7 (phenyl ring atoms). Cg9 is defined by atoms C92, C102–C142 (phenyl ring atoms) in L7

[b] Cg···P1 is the perpendicular distance of corresponding centroid to a plane. Planes P1 or P2 are defined by the atoms, which define the corresponding centroids

[c] Cg···P2 is the perpendicular distance of corresponding centroid to a plane. Planes P1 or P2 are defined by the atoms, which define the corresponding centroids

[d] Dihedral angle between P1 and P2

[e] Angle between Cg···Cg distance and Cg···P1

[i] = x,−1 + y, z

[ii] = x,1 + y, z

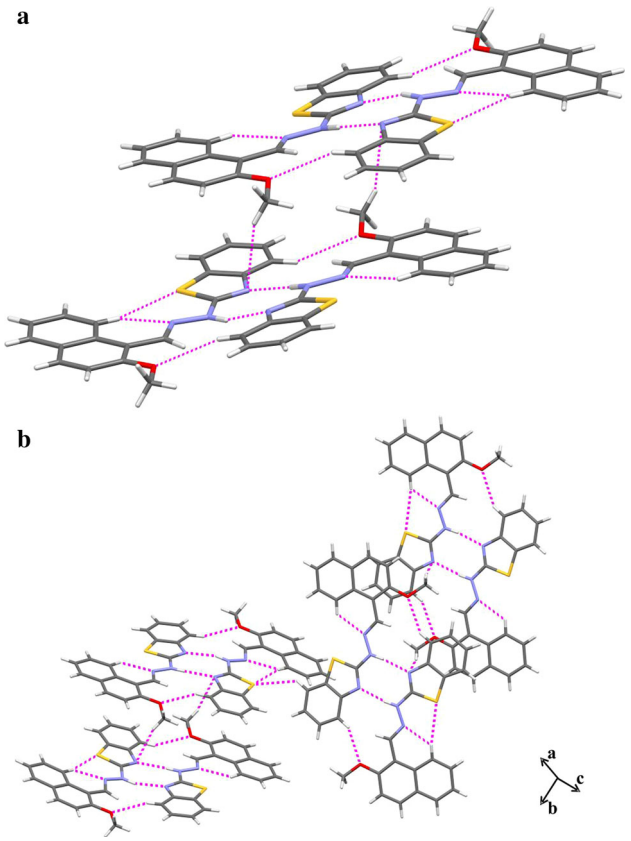

Fig. 3 **a** Structural motif of compound L7 generated via N–H···N, C–H···O, C–H···N and C–H···S hydrogen bonds (shown as *dashed magenta lines*). **b** Part of crystal packing of L7 showing mutually connected dimers via weak C–H···N and C–H···S hydrogen bonds

4-methoxy-1-naphthaldehyde-(2-benzothiazolylhydrazone) (L8)

Weak intramolecular C15–H11···N3 hydrogen bond shapes *S*(6) structural motif, similar to compound L7. Molecules of compound L8 are connected via intermolecular N2–H12 N···N1 and C19–H19B···O1 hydrogen bonds (Table 4), respectively, into alternating $R_2^2(8)$ and $R_2^2(6)$ centrosymmetric rings which further form 2D layers (Fig. 4a). These layers are perpendicularly supported by π–π interactions between the thiazolyl and phenyl rings (Fig. 4b, Table 5).

6-methoxy-2-naphthaldehyde-(2-benzothiazolylhydrazone) (L9)

Intramolecular hydrogen bonds are not found in compound L9. Similar to crystal structure of compound L7, crystallographically independent molecules 1 and 2 in asymmetric unit of compound L9 are mutually connected into $R_2^2(8)$ dimers via intermolecular N21–H21 N···N12 and N22–H22 N···N11 hydrogen bonds (Table 4). Interestingly, molecules 2 are mutually connected via C42–H42···O12 hydrogen bond into $C_1^1(16)$ chains which is not the case for molecules 1 (Fig. 5).

Antiproliferative effects in vitro

We evaluated antiproliferative effects of L1–L9 on human tumor cell lines, as well as cytotoxicity on mouse embryonic fibroblasts. All tested ligands exerted strong antiproliferative effects on tumor cells and cytotoxic effects on

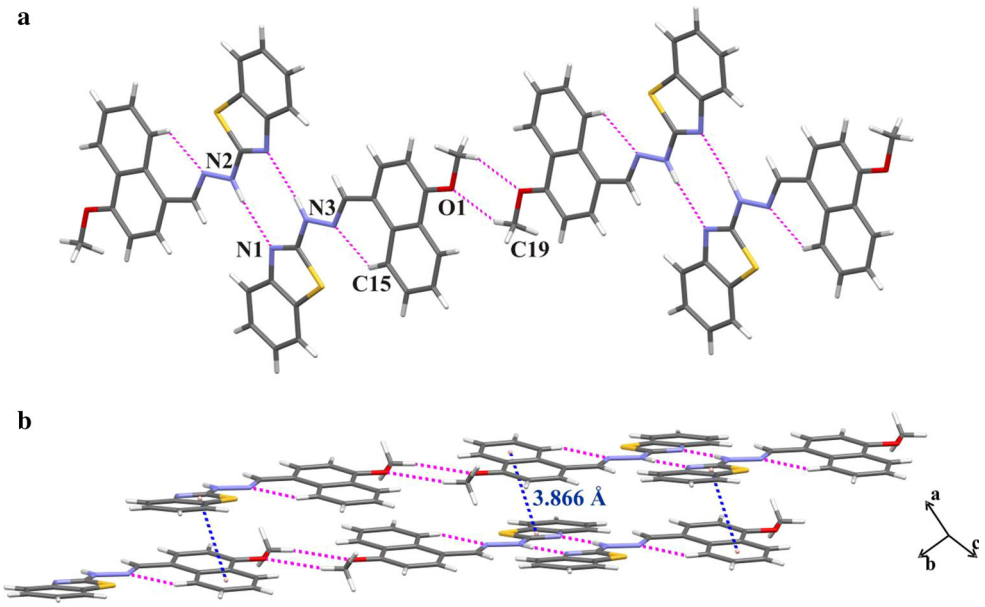

Fig. 4 **a** Main supramolecular motif in compound L8 shaped via N2–H12 N···N1 and C19–H19B···O1 hydrogen bonds shown as *dashed magenta lines*. **b** Alternating $R_2^2(8)$ and $R_2^2(6)$ centrosymmetric rings shaped via N2–H12 N···N1 and C19–H19B···O1 hydrogen bonds into 2D layers (shown as *dashed magenta lines*) that are supported by weak aromatic stacking interaction between the thiazolyl and phenyl rings of adjacent chains (shown as *dashed dark blue lines*)

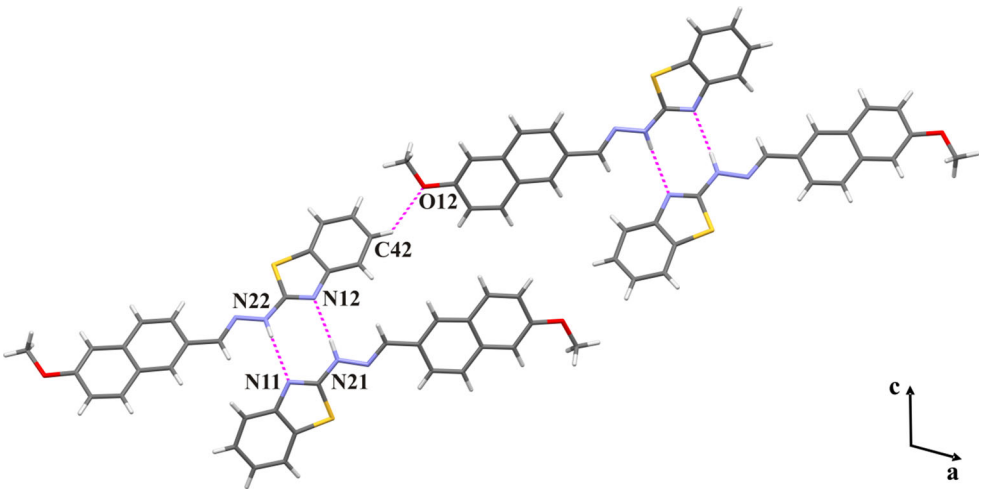

Fig. 5 Part of crystal structure of L9 showing $R_2^2(8)$ dimers formed via intermolecular N21–H21 N···N12 and N22–H22 N···N11 hydrogen bonds and $C_1^1(16)$ chains formed via C42–H42···O12 hydrogen bond (shown as *dashed magenta lines*)

Table 6 IC_{50} values (μM)

Substance	IC_{50}^{a} (μM)				
	Cell lines				
	SW620	A549	HepG2	3T3	HeLa
L1	8.16	6.72	8.17	5.59*	5.20
L2	9.08	9.63	>100	4.05	5.0*
L3	7.19	5.74	7.57	4.55	6.50
L4	6.44*	6.97*	>100*	7.79*	6.44*
L5	3.30*	5.20*	3.54*	1.98*	4.08*
L6	49.08	8.31	6.34	>100*	6.94
L7	89.74	9.71	52.05	>100	78.56
L8	32.47	41.04	26.16	18.18	30.51
L9	4.20	2.56	3.87	<0.01	>100

[a] IC_{50}; 50 % inhibitory concentration or compound concentration required to inhibit tumor cell proliferation by 50 %

* The color of the substance interferes with colorimetric measurements at the highest tested concentration (100 μM)

Table 7 Calculated standard Gibbs energies of binding at 298.15 K and 1 atm for dimers or tetramers of L1–L9 (B3LYP/6-311 ++G(d,p) level of the theory)

Substance	$\Delta_r G^{\circ}_{binding}$/kJ mol^{-1}
L1	−139.76
L2	–
L3	–
L4	–
L5	–
L6	−99.61
L7	−110.78
L8	−86.20
L9	−96.24

fibroblasts with exception of L6 and L7 that had no effect on fibroblast cells (Table 6). Compounds L7 and L8 are the least potent ligands and inhibited tumor cell growth at higher tested concentrations (10–1000 μM). Compounds L1–L5 and L9 had non-selective strong antiproliferative effects, on all tested cells at micromolar concentration (<1 μM) except for L4 that had no effect on HepG2 and L9 that had no effects on HeLa cells.

Quantum chemical calculations

Standard Gibbs energies of binding were calculated by subtraction of standard Gibbs energies of formation for monomers from the standard Gibbs energies of dimers or tetramers. These values revealed that the stability in L6 and L7 is bigger than in L8 (Table 7). In L7, the existence of weak C51–H51···O12 and C52–H52···O11 hydrogen bonds that form $R_2^2(22)$ rings was already mentioned previously. Since L6 and L7 have the oxygen atom attached to the same position 2, it is reasonable to predict that this position is more favorable for binding due to the formation of two weak hydrogen bonds. On the contrary, in L8 where the oxygen atom of methoxy group is attached in position 4, there is no such a possibility and consequently the structure is less stable. Moreover, the methoxy group provides better stabilization of dimers than the hydroxyl group (Table 7). Since the experimental structures of L2–L5 are not available, the stability of L1 was not compared to any value.

In order to deeply understand the cause of molecular packing in investigated systems, we calculated the potential energy surfaces of molecules spanned by torsional coordinates (Scheme 2, Fig. S28). Changes along these torsional coordinates could produce different conformers that will pack diverse unit cell and therefore are important for explanation of structures. Calculation of PES scans

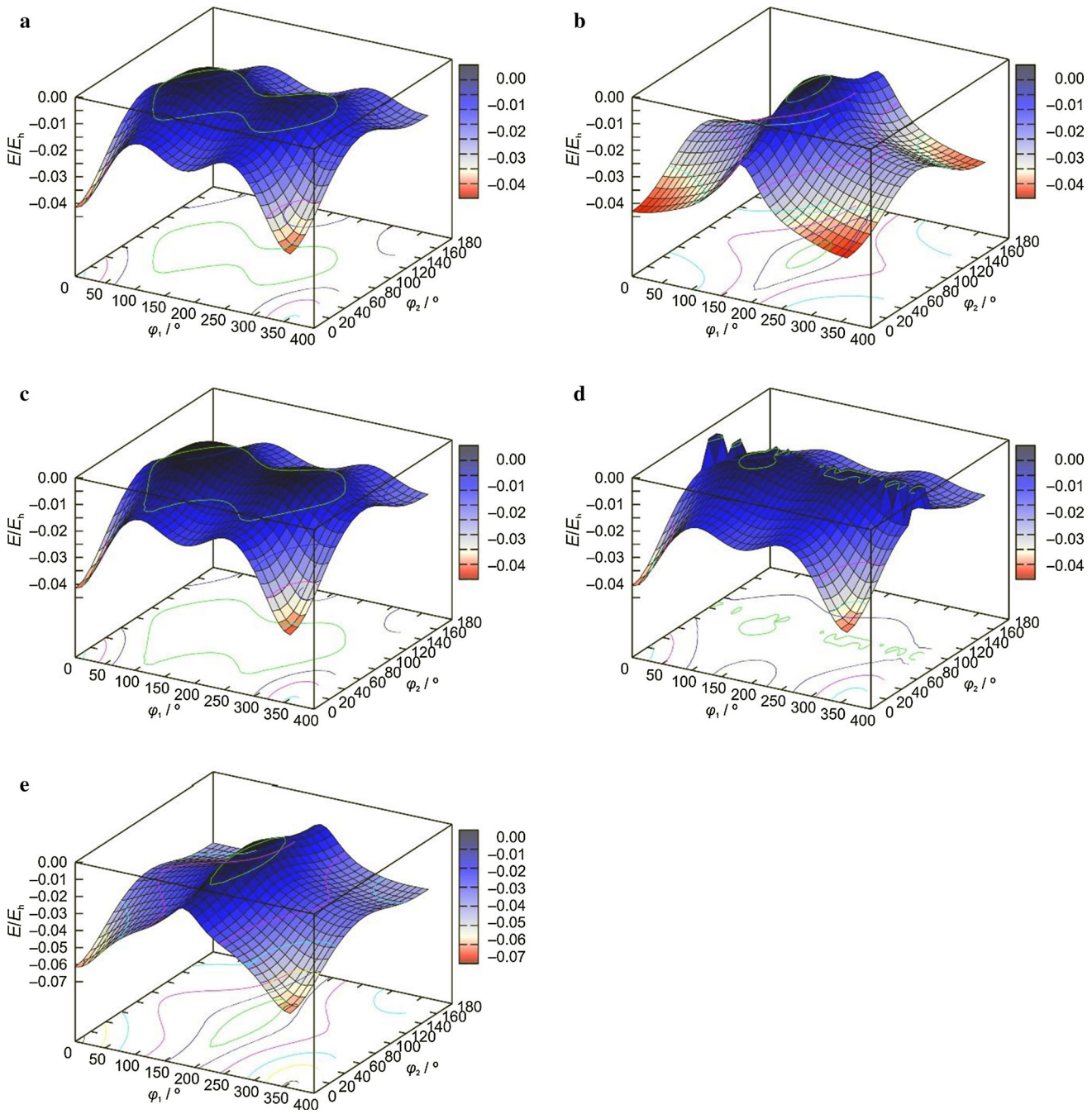

Fig. 6 Potential energy surfaces spanned by two torsional coordinates φ_1 and φ_2 (defined on Scheme 2): **a** L1, **b** L2, **c** L3, **d** L4, and **e** L5

along the two torsional coordinates shows that the internal rotation in L1 is very unfavorable due to the presence of intramolecular hydrogen bond (Fig. 6a, for $\varphi_1 = 0°$). Although along this PES slice there is another local minimum, this structure is much higher in energy to be able to produce packing. Potential energy surfaces calculated for compounds L2–L5 (Fig. 6b–e) are showing the similar behavior, and it is reasonable to predict that the packing of all these compounds will be similar.

Internal rotation curves of naphthalene rings in L6, L7, L8, (Fig. 7) and L9 (Fig. 8) show that the conformers of minimal energy are the ones where this ring is on the same side as lone electronic pair of imine nitrogen atom, which is exactly the same as in obtained crystal structures.

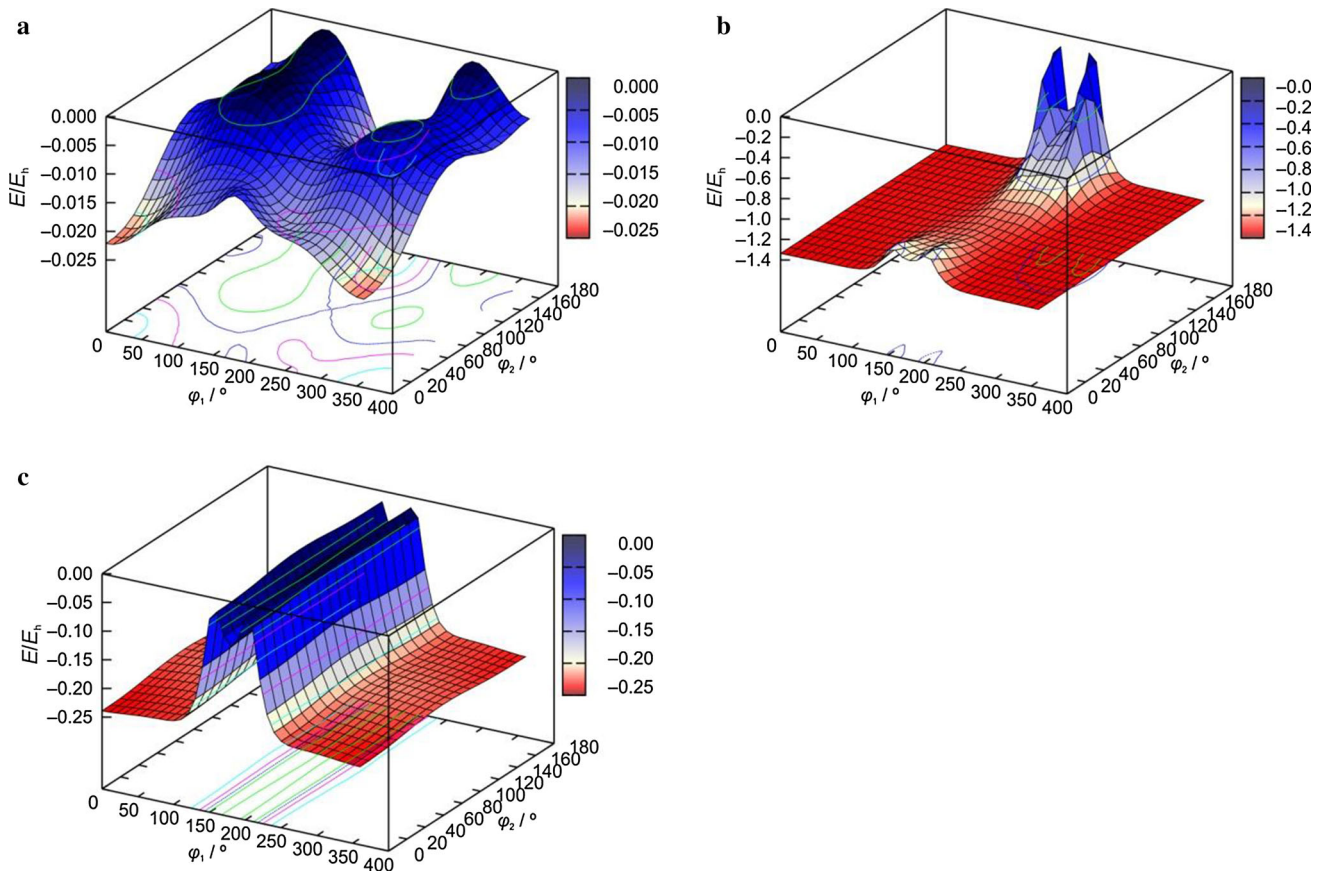

Fig. 7 Potential energy surfaces spanned by two torsional coordinates φ_1 and φ_2 (defined on Scheme 2): **a** L6, **b** L7, and **c** L8

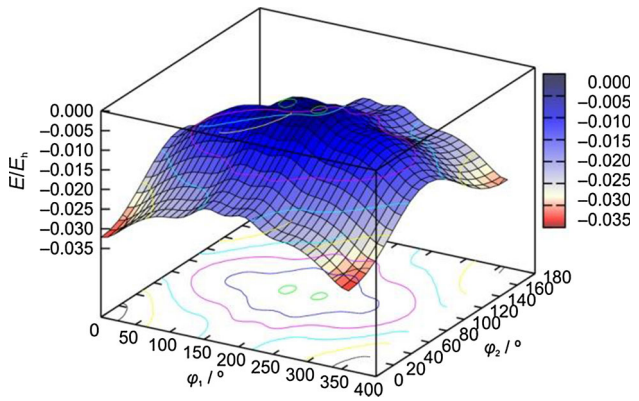

Fig. 8 Potential energy surfaces spanned by two torsional coordinates φ_1 and φ_2 (defined on Scheme 2) for L9

Conclusions

In our aims to prepare metal complexes with 2-benzothiazolylhydrazone ligands and investigate their pharmacological activities, we firstly synthesized and characterized a series of nine 2-benzothyazolylhydrazone ligands (L1–L9) functionalized by $-$OH or $-OCH_3$ functionalities at different phenyl or naphthyl positions and investigated their potential biological activities. The compounds L1–L9 are characterized by elemental analysis, IR and NMR spectroscopy, and compounds L1, L7–L9 are structurally determined in the solid state by single-crystal X-ray diffraction method.

In all 2-benzothiazolylhydrazones derived form 2-methoxy-1-naphthaldehyde, 4-methoxy-1-naphthaldehyde and 6-methoxy-2-naphthaldehyde (L7–L9, respectively) characteristic $R_2^2(8)$ dimer is shaped via $N_{hydrazino}$–H···$N_{thiazolyl}$ intermolecular hydrogen bond, but these dimers are differently supported ($R_2^2(22)$ fused rings in L7, alternating $R_2^2(8)$ and $R_2^2(6)$ centrosymmetric rings in L8 and $C_1^1(16)$ infinite chains in L9) by C–H···O intermolecular hydrogen bonds which are formed via $-OCH_3$ group. On the contrary to the amino L7–L9 dimer arrangements of primary crystal structure, supramolecular structure of imino L1 hydrazone is shaped into infinite helical $C(4)$ chains along b axis via $N_{thiazolyl}$–H···$N_{hydrazino}$ intermolecular hydrogen bond.

Moreover, quantum chemical calculations confirmed that methoxy group (L7–L9) provides better stabilization of dimers than the hydroxyl group in the L1 hydrazone which prefers formation of intramolecular O–H···N hydrogen bond over intermolecular ones. Calculated

standard Gibbs energies of formation reveal that oxygen atom attached to the position 2 in L6 and L7 is more favorable for binding than the position 4 (L8). Potential energy surfaces calculated for compounds L2–L5 are showing the similar behavior to compound L1, and it is reasonable to predict that the packing of all these compounds will be similar.

All tested ligands exerted strong antiproliferative effects on tumor cells and cytotoxic effects on fibroblasts except L6 and L7 that had no effect on fibroblast cells. Compounds L7 and L8, characterized by methoxy-substituted 1-naphthyl moiety, were the least potent ligands. Compound L9, characterized by methoxy-substituted 2-naphthyl moiety, and compounds L1–L5, characterized by hydroxy-substituted phenyl moiety, exerted non-selective strong antiproliferative effects on all tested cells at micromolar concentrations.

Acknowledgments We acknowledge Krešimir Molčanov, PhD, Division of Physical Chemistry, Laboratory for chemical and biological crystallography, Ruđer Bošković Institute, Zagreb, Croatia, for X-ray single-crystal diffraction data collection for compound **8**. We greatly appreciate support of University of Rijeka research Grant No. 13.11.1.1.11 and access to equipment in possession of University of Rijeka within the project "Research Infrastructure for Campus-based Laboratories at University of Rijeka", financed by European Regional Development Fund (ERDF).

References

1. Mortimer CG, Wells G, Crochard JP, Stone EL, Bradshaw TD, Stevens MFG, Westwell AD (2006) J Med Chem 49:179–185
2. Al-Tel TH, Al-Qawasmeh RA, Zaarour R (2011) Eur J Med Chem 46:1874–1881
3. Ćaleta I, Kralj M, Marjanović M, Bertosa B, Tomić S, Pavlović G, Pavelić K, Karminski-Zamola G (2009) J Med Chem 52:1744–1756
4. Pattan SR, Suresh C, Pujar VD, Reddy VVK, Rasal VP, Koti BC (2005) Indian J Chem 44:2404–2408
5. Siddiqui N, Pandeya SN, Khau SA, Stables J, Rana A, Alam M, Arshad MF, Bhat MA (2007) Bioorg Med Chem Lett 17:255–259
6. Gurupadayya BM, Gopal M, Padmashali B, Vaidya VP (2005) Ind J Heterocycl Chem 15:169–172
7. Pavlović G, Racané L, Čičak H, Tralić-Kulenović V (2009) Dyes Pigments 83:354–362
8. Allen FH (2002) Acta Crystallogr B58:380–388
9. Groom CR, Bruno IJ, Lightfoot MP, Ward SC (2016) Acta Crystallogr B72:171–179
10. Lindgren EB, Yoneda JD, Leal KZ, Nogueira AF, Vasconcelos TRA, Wardell JL, Wardell AMV (2013) J Mol Struct 1036:19–27
11. Nogueira AF, Vasconcelos TRA, Wardell JL, Wardell SMSV (2011) Z Kristallogr 226:846–860
12. Vanucci-Bacqué C, Carayon C, Bernis C, Camare V, Nègre-Salvayre A, Bedos-Belval F, Baltas M (2014) Bioorg Med Chem 22:4269–4276
13. Patil SA, Weng CM, Huang PC, Hong FE (2009) Tetrahedron 65:2889–2897
14. Lindgren EB, de Brito MA, Vasconselos TRA, de Morales MO, Montenegro RC, Yoneda JD, Leal KZ (2014) Eur J Med Chem 86:12–16
15. Girish SR, Revankar VK, Mahale VB (1996) Transit Met Chem 21:401–405
16. X'Pert Sofware Suite, Version 1.3e, Panalytical B.V., Almelo, The Netherlands, 2001
17. Vreshch V (2011) J Appl Crystallogr 44:219–220
18. Oxford Diffraction Ltd., Xcalibur CCD system, CrysAlis Software system Versions 1.171.37.35. Abingdon, Oxfordshire, England, 2008
19. Sheldrick GM (2008) Acta Crystallogr Sect A64:112–122
20. Farrugia LJ (1999) J Appl Crystallogr 32:837–838
21. Spek L (2003) J Appl Crystallogr 36:7–13
22. Macrae CF, Bruno IJ, Chisholm JA, Edgington PR, McCabe P, Pidcock E, Rodriguez-Monge L, Taylor R, van de Streek J, Wood PA (2008) J Appl Crystallogr 41:466–470
23. Becke AD (1993) J Chem Phys 98:5648–5652
24. Lee C, Yang W, Parr RG (1998) Phys Rev B 37:785–789
25. Grimme S, Ehrlich S, Goerigk L (2011) J Comput Chem 32:1456–1465
26. Hrenar T (2014) qcc, Quantum Chemistry Code, rev. 0.68
27. Primožič I, Hrenar T, Baumann K, Krišto L, Križić I, Tomić S (2014) Croat Chem Acta 87:155–162
28. Hrenar T, moonee, Code for manipulation and analysis of multi- and univariate data, rev. 0.6826, 2014
29. Gaussian 09, Revision E.01, Frisch MJ, Trucks GW, Schlegel HB, Scuseria GE, Robb MA, Cheeseman JR, Scalmani G, Barone V, Mennucci B, Petersson GA, Nakatsuji H, Caricato M, Li X, Hratchian HP, Izmaylov AF, Bloino J, Zheng G, Sonnenberg JL, Hada M, Ehara M, Toyota K, Fukuda R, Hasegawa J, Ishida M, Nakajima T, Honda Y, Kitao O, Nakai H, Vreven T, Montgomery Jr JA, Peralta JE, Ogliaro F, Bearpark M, Heyd JJ, Brothers E, Kudin KN, Staroverov VN, Kobayashi R, Normand J, Raghavachari K, Rendell A, Burant JC, Iyengar SS, Tomasi J, Cossi M, Rega N, Millam JM, Klene M, Knox JE, Cross JB, Bakken V, Adamo C, Jaramillo J, Gomperts R, Stratmann RE, Yazyev O, Austin AJ, Cammi R, Pomelli C, Ochterski JW, Martin RL, Morokuma K, Zakrzewski VG, Voth GA, Salvador P, Dannenberg JJ, Dapprich S, Daniels AD, Farkas Ö, Foresman JB, Ortiz JV, Cioslowski J, Fox DJ (2009) Gaussian Inc., Wallingford, CT. http://www.gaussian.com/g_tech/g_ur/m_citation.htm
30. Gvozdjakova A, Ivanovičova H (1986) Chem Papers 40:797–800
31. Easmon J, Heinisch G, Holzer W (1989) Heterocycles 29:1399–1408
32. Easmon J, Puerstinger G, Roth T, Fiebig HH, Jenny M, Jaeger W, Heinisch G, Hofmann J (2001) Int J Cancer 94:89–96